Enhanced association and dissociation of heteronuclear Feshbach molecules in a microgravity environment

J. P. D'Incao,[1,2] M. Krutzik,[3,4] E. Elliott,[4] and J. R. Williams[4]
[1]*JILA, University of Colorado and NIST, 440 UCB, Boulder, Colorado 80309, USA*
[2]*Department of Physics, University of Colorado, Boulder, Boulder, Colorado 80302, USA*
[3]*Humboldt-Universität zu Berlin, Institut für Physik, Newtonstr. 15, 12489 Berlin, Germany*
[4]*Jet Propulsion Laboratory, California Institute of Technology, 4800 Oak Grove Drive, Pasadena, California 91011, USA*
(Received 15 July 2016; published 3 January 2017)

We study the association and dissociation dynamics of weakly bound heteronuclear Feshbach molecules using transverse radio-frequency fields for expected parameters accessible through the microgravity environment of NASA's Cold Atom Laboratory (CAL) aboard the International Space Station, including subnanokelvin temperatures and atomic densities as low as $10^8/\mathrm{cm}^3$. We show that under such conditions, thermal and loss effects can be greatly suppressed, resulting in a high efficiency of both association and dissociation of Feshbach molecules with a mean size exceeding $10^4 a_0$ and allowing for the coherence in atom-molecule transitions to be clearly observable. Our theoretical model for heteronuclear mixtures includes thermal, loss, and density effects in a simple and conceptually clear manner. We derive the temperature, density, and scattering length regimes of ^{41}K-^{87}Rb that allow optimal association or dissociation efficiency with minimal heating and loss to guide upcoming experiments with ultracold atomic gases in space.

DOI: 10.1103/PhysRevA.95.012701

I. INTRODUCTION

Association and dissociation of ultracold Feshbach molecules have been enabling probes of fundamental physics throughout the last decade [1,2]. Produced near Feshbach resonances where the atomic s-wave scattering length a is magnetically tunable, these molecules have large spatial extents and extremely weak binding energies. Feshbach molecules formed in Fermionic gases were crucial in the exploration of BEC-BCS crossover physics [3–11]. Their heteronuclear counterparts are important ingredients for the creation of ultracold polar molecules [12–22] and can be used to study universal few-body phenomena [23–29]. Additionally, Feshbach molecules can be used as sources of entangled states [30–40] or to test for variations of fundamental constants with unprecedented sensitivity [41–44].

Microgravity offers several fundamental advantages for the study of cold atoms, which has sparked growing interest [45–47] and high-profile experimental efforts [48–50]. First and most prominently, ultracold atoms released into microgravity enable interrogation and observation times orders of magnitude longer than their earthbound counterparts, even in a compact setup, laying the foundation for the next generation of space-based atom interferometer sensors for both fundamental and applied physics applications [51–53]. Second, the removal of a linear gravitational potential allows for enhanced delta-kick cooling and adiabatic decompression to conserve the phase-space density while lowering both the temperature and the density [54–57], opening the door to a new parameter regime of ultralow densities and ultracold temperatures. Finally, microgravity negates the "gravitational sag" that gives a mass-dependent displacement of ultracold gases from their trap centers [58,59], limiting the overlap of multiple, distinct atomic species prepared at low temperatures in a common trap. Eliminating this sag removes a dominant systematic error in equivalence principle measurements that use dual-species atomic clouds as quantum test masses [52,53,60]. Therefore, the unique environment of space provides a means to study high phase-space densities of single- or multispecies gases in new regimes of temperature and density held by vanishingly weak traps or even in extended free fall.

To this end, NASA's Cold Atom Laboratory (CAL) is scheduled for launch in 2017 as a multiuser facility of the International Space Station (ISS) to study ultracold atoms, dual-species mixtures, and/or quantum degenerate gases of bosonic ^{87}Rb and ^{39}K or ^{41}K in persistent microgravity [61]. CAL is designed as a simple, yet versatile, experimental facility that features numerous core technologies for contemporary quantum gas experiments including tunable magnetic fields [steady state, radio frequency (RF), and microwave] for atomic-state manipulation and access to homonuclear or heteronuclear Feshbach resonances, Bragg beams for dual-species atom interferometry, and high-resolution absorption imaging capabilities.

In this paper we develop a simple and intuitive description of the association and dissociation of heteronuclear Feshbach molecules using oscillating magnetic fields. We further apply this general treatment to ^{41}K-^{87}Rb molecules within the microgravity regime at CAL. Note that our model does not explicitly incorporate many-body effects, as these corrections should not qualitatively alter the results in the ultralow temperature and density regimes relevant to CAL. However, our results highlight the coherent properties of association and dissociation of Feshbach molecules and qualitatively include the effects of density, temperature, and few-body losses. Our results are consistent with previous experiments performed at the usual temperatures and densities relevant for terrestrial experiments [62,63]. We find that the efficiency of association and dissociation of extremely weakly bound Feshbach molecules are greatly enhanced in the CAL environment, allowing for observation of their coherent properties with a high accuracy and minimal incoherent effects associated with heating and losses. From our analysis, we identify the conditions (in terms of the experimentally relevant parameters)

a system needs to satisfy in order to achieve a high efficiency of both association and dissociation.

II. MOLECULAR ASSOCIATION AND DISSOCIATION

The use of RF fields for association and dissociation of Feshbach molecules [64–66], as well as for the control of interatomic interactions [67–70], is today one of the most widely applied tools in ultracold atomic and molecular gases since it provides an exquisite accuracy in revealing details of the interactions and dynamics [1,2]. The scheme we employ for Feshbach molecule association and dissociation uses an oscillating RF magnetic field (transversal to the direction of the main Feshbach field) which couples atomic hyperfine states whose $\Delta m_f = \pm 1$, where m_f is the azimuthal component of the hyperfine angular momentum f. Provided that the magnetic-field modulation frequency, $\omega/2\pi$, is resonant with a single hyperfine transition for one of the species (i.e., no other hyperfine states are nearby), the interaction that defines the coupling between the relevant states can be stated as

$$W(t) = \frac{\hbar\Omega}{2}(|\alpha\rangle\langle\alpha'| + |\alpha'\rangle\langle\alpha|)\cos\omega t, \tag{1}$$

where $\Omega/2\pi$ is the atomic Rabi frequency, while $|\alpha\rangle \equiv |f_\alpha m_{f_\alpha}\rangle$ and $|\alpha'\rangle \equiv |f_{\alpha'} m_{f_{\alpha'}}\rangle$ are the two hyperfine states satisfying the condition $\Delta m_f = m_{f_\alpha} - m_{f'_\alpha} = \pm 1$. One interesting aspect of this scheme is that it allows for choosing the free-atom initial state in a weakly interacting spin state at magnetic fields near the Feshbach resonance, avoiding large three-body losses that otherwise arise for resonantly interacting bosonic gases. Relevant to CAL, an initial weakly interacting mixture of Rb and K atoms in the $|10\rangle$ and $|11\rangle$ states, respectively, would be available to access Feshbach molecules in the $|11\rangle$ atomic states of both species at magnetic fields near the broad resonance at 39.4 G [63,71–73]. However, we keep our theoretical model general.

Our model for molecular association and dissociation is derived from the Floquet formalism [74], appropriate for time-periodic Hamiltonians, and assumes zero-range interatomic interactions [75]. Although more sophisticated theoretical models exist [1,2], the use of zero-range interactions will allow us to extract the important parameters controlling the various aspects of molecular association and dissociation relevant for experiments. Within our framework, the Floquet Hamiltonian for two atoms in the presence of an external field (periodic in time) is written as

$$\mathscr{H}_F = H + |\beta\rangle W(t)\langle\beta| - i\hbar\frac{\partial}{\partial t}, \tag{2}$$

where H is the bare, time-independent, two-atom Hamiltonian whose eigenstates are ψ_ν with energies E_ν, and $|\beta\rangle$ is the internal state for the spectator atom, i.e., the atom not affected by the external field. We seek the solutions of the Floquet Schrödinger equation, $\mathscr{H}_F\Psi_F = \varepsilon\Psi_F$, with quasieigenenergy ε and quasieigenstate

$$\Psi_F(\vec{r},t) = \sum_{n\nu} c_\nu^n \psi_\nu(\vec{r}) e^{in\omega t}. \tag{3}$$

In the above equation, $\vec{r}$ is the interparticle vector, and n is the photon number. Considering only s-wave interactions, the bare wave function can be written as

$$\psi_\nu(\vec{r}) = \frac{1}{2}\sqrt{\frac{1}{\pi}}\frac{f_\nu(r)}{r}|S_\nu\rangle, \tag{4}$$

where $|S_\nu\rangle = \{|\alpha\beta\rangle, |\alpha'\beta\rangle\}$ represents the two-atom spin states and f_ν is their corresponding radial wave function. Now, using Eq. (3) we can write the Floquet Schrödinger equation, after projecting out the base $\psi_\nu(\vec{r})e^{in\omega t}$, as

$$\sum_{n'\nu'}\Bigg[E_\nu\delta_{nn'}\delta_{\nu\nu'} + \frac{\hbar\Omega^\nu_{\nu'}}{2}(\delta_{n,n'+1} + \delta_{n+1,n'}) + (n\hbar\omega - \varepsilon)\delta_{nn'}\delta_{\nu\nu'}\Bigg]c^{n'}_{\nu'} = 0, \tag{5}$$

where

$$\Omega^\nu_{\nu'} = \Omega\int_0^\infty f^*_\nu(r) f_{\nu'}(r) dr \tag{6}$$

defines the two-atom Rabi frequency. Note that $\Omega^\nu_{\nu'}$ is nonzero only for values of $\nu \neq \nu'$ satisfying the selection rules ($\Delta m_f = \pm 1$) imposed by the form of the atom-external field coupling in Eq. (1). The solutions of Eq. (5) fully determine the time evolution of the atomic and molecular states coupled by the external field. In practice, for values of $\hbar\Omega^\nu_{\nu'} \ll |E_\nu - E_{\nu'}|$, only states with $|n| = 0$ and 1 are necessary to accurately describe the system.

For the present study, atoms in spin state $|\alpha\beta\rangle$ are unbound, while atoms in the $|\alpha'\beta\rangle$ state are bound in the Feshbach molecule. (Note that we denote the corresponding states for atoms in spins $|\alpha\beta\rangle$ and $|\alpha'\beta\rangle$ as $\nu \equiv k$ and $\nu \equiv m$, respectively.) In this case, the two-atom Rabi frequency, (6), is determined from the wave functions

$$f_k(r) = \sqrt{\frac{2\mu\epsilon_r}{\pi\hbar^2 k}}\sin(kr - ka'), \tag{7}$$

$$f_m(r) = \sqrt{\frac{2}{a}}e^{-r/a}, \tag{8}$$

where μ is the two-body reduced mass, $k^2 = 2\mu E/\hbar^2$ (E is the collision energy), and a and a' are the scattering lengths for atoms in the $|\alpha'\beta\rangle$ and $|\alpha\beta\rangle$ spin states, respectively. Note that in Eq. (7) we have introduced an arbitrary energy scale, ϵ_r. Our primary motivation for writing the collisional wave function as in Eq. (7) is that it preserves the usual energy-normalized form of a scattering state and, therefore, leads to scattering properties obeying their proper Wigner threshold laws. In our approach, the necessity of the introduction of a new energy scale originates from a simple inspection of Eq. (6): f_k needs to have units of $1/\text{length}^{1/2}$ and that can be accomplished by introducing ε_r. We set $\epsilon_r = \epsilon_{\text{Rb}} + \epsilon_{\text{K}}$, where $\epsilon_i = \hbar^2(6\pi^2 n_i)^{2/3}/2m_i$ is the Fermi energy (characterizing the average local energy of the gas), with n_i and m_i being the density and mass of the atomic species i, respectively. This allows our model to qualitatively account for density effects in a physically meaningful way. [For instance, one can show that with ϵ_r set in this way the integral of f_k^2 up to the average interatomic distance ($n^{-1/3}$) is proportional to $n^{1/3}/k$, i.e., the ratio between the de Broglie wavelength and the average interatomic distance.] Similar ways to qualitatively account for density effects have been successfully used in

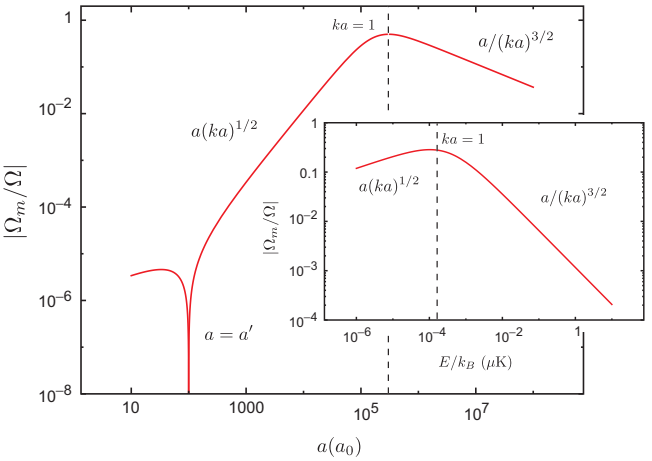

FIG. 1. Molecular Rabi frequency $\Omega_m/2\pi$ (in units of the atomic Rabi frequency, $\Omega/2\pi$) as a function of the scattering length. For this calculation we used $n_{\rm Rb} = n_{\rm K} = 10^8/{\rm cm}^3$, $a' = 100a_0$, and $E/k_B = 100$ pK. Inset: Energy dependence of Ω_m/Ω assuming $a = 10^5 a_0$.

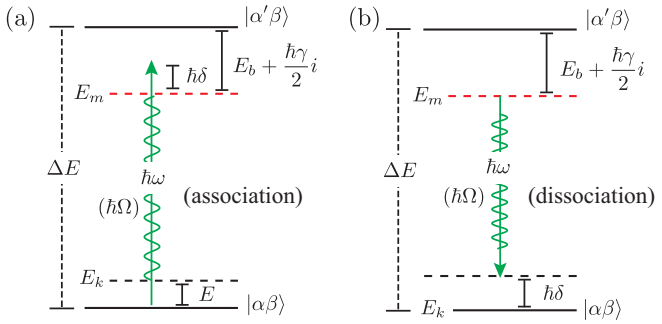

FIG. 2. Schematic of our present level scheme for (a) molecular association and (b) molecular dissociation. Here, ΔE is the energy difference between the relevant two-atom thresholds, $|\alpha\beta\rangle$ and $|\alpha'\beta\rangle$, $E_b = \hbar^2/2\mu a^2$ is the molecular binding energy, γ is the molecular lifetime (see text), and E is the energy of the two atoms in the $|\alpha\beta\rangle$ state. Atomic and molecular states are coupled via an external field with frequency $\omega/2\pi$ (with detuning δ) and Rabi frequency $\Omega/2\pi$. E_K and E_m are given in Eq. (10).

few-body models [76–80] in order to explain molecular formation and other important properties relevant for ultracold gas experiments.

Having established the form of the wave function for the relevant states, we can now substitute Eqs. (7) and (8) into Eq. (6), in order to obtain the molecular Rabi frequency $\Omega_m \equiv \Omega_m^k$,

$$\Omega_m(k) = \Omega\sqrt{\frac{4\mu\epsilon_r}{\pi\hbar^2}}\frac{(a-a')}{(1+k^2a^2)}(ka)^{1/2}. \tag{9}$$

We obtained this result within the limit of $ka' \ll 1$, assumed for a weakly interacting scattering state in Eq. (7), and neglecting corrections of the order of $(ka')^2$. As one can see, due to the dependence on ϵ_r, the molecular Rabi frequency is also density dependent ($\Omega_m \sim n^{1/3}$). In Fig. 1 we show the ratio of the molecular to atomic Rabi frequencies (Ω_m/Ω) as a function of both the scattering length and the energy (inset) and indicate the low- and high-energy behavior, i.e., $ka \ll 1$ [$\Omega_m \propto a(ka)^{1/2}$] and $ka \gg 1$ [$\Omega_m \propto a/(ka)^{3/2}$], respectively.

We now have defined all elements necessary to solve Eq. (5). As mentioned above, in the regime of small $\hbar\Omega_m$, we need only consider states with $|n| = 0$ and 1. Therefore, including only the states $\{\nu,n\} = \{k,0\}$ and $\{m,-1\}$, the eigenvalue equation, (5), reduces to

$$\begin{pmatrix} E_k & \frac{\hbar\Omega_m}{2} \\ \frac{\hbar\Omega_m}{2} & E_m - \hbar\omega \end{pmatrix}\begin{pmatrix} c_k^0 \\ c_m^{-1} \end{pmatrix} = \varepsilon\begin{pmatrix} c_k^0 \\ c_m^{-1} \end{pmatrix}, \tag{10}$$

which is formally equivalent to a two-level system in the presence of an external field within the rotating-wave approximation, whose solutions are well known [81]. The solutions are expected to be accurate provided $\hbar\Omega_m \ll |E_k - E_m|$ (see Fig. 2 for a schematic of the level scheme considered), therefore covering the parameter regime explored in our studies. As we see next, the fact that these levels now represent a bound molecular state and two-atom continuum state makes it important to include thermal and loss effects in order to determine the time evolution process leading to association and dissociation of weakly bound molecules. We also note that our effective two-level model [a bound and a single continuum state, Eqs. (8) and (7), respectively] incorporates effects of other continuum states only to the extent that our results are thermally averaged. As a result, our model should be valid for times shorter than $2\pi/\Omega_m$—all our studies were performed within this regime—and does not describe energy shifts of the dressed molecular state [1]. Such shifts, however, should not affect our studies of the coherent properties of association and dissociation and the determination of the relevant parameter regime in which they are most pronounced.

The molecular association scheme, which couples atomic and molecular states with different m_f values, is illustrated in Fig. 2(a). Here, $E_k = E$ and $E_m = \Delta E - E_b - i\hbar\gamma/2$, where $E_b = \hbar^2/2\mu a^2$ is the binding energy of the molecular state and $\hbar\gamma$ is its corresponding width, introduced here to account for the finite lifetime of the molecular state due to collisions with other atoms and molecules. This model is valid for times shorter than $1/\gamma$. Assuming that at $t = 0$ the atoms are unbound ($\nu = k$), the probability of finding the atoms in the molecular state ($\nu = m$) at later times, $t = \tau$, is given by the probability associated with the linear combination of the eigenstates of Eq. (10), including the corresponding phase evolution $e^{-i\varepsilon t/\hbar}$, satisfying the initial condition at $t = 0$. In this case, we obtain

$$P_m(E,\tau) = e^{-\gamma\tau/2}\left(\frac{\Omega_m}{\Omega_{\rm eff}^m}\right)^2\left|\sin\left(e^{i\theta_m}\frac{\Omega_{\rm eff}^m\tau}{2}\right)\right|^2, \tag{11}$$

where

$$\Omega_{\rm eff}^m = \left\{\gamma^2\left(\delta + \frac{E}{\hbar}\right)^2 + \left[\Omega_m^2 + \left(\delta + \frac{E}{\hbar}\right)^2 - \frac{\gamma^2}{4}\right]^2\right\}^{\frac{1}{4}}, \tag{12}$$

$$\theta_m = \frac{1}{2}\tan^{-1}\left[\frac{\left(\delta + \frac{E}{\hbar}\right)\gamma}{\Omega_m^2 + \left(\delta + \frac{E}{\hbar}\right)^2 - \frac{\gamma^2}{4}}\right]. \tag{13}$$

Here, $\hbar\delta$ is the energy detuning from the molecular transition in Fig. 2(a). Note that even for $\delta = 0$—where one would expect the system to be on resonance—finite energy and

molecular decay effects can lead to an effective detuning through Eqs. (12) and (13). Note also that $dP_m/d\tau$ in the limit $\tau \to 0$ is related to the transition rate derived in Ref. [64] based on Fermi's Golden Rule. It is important to emphasize here that for the process of molecular association, since there exists a thermal distribution of initial states [65], the transition probability needs to be thermally averaged according to

$$\langle P_m(T,\tau)\rangle = \frac{2}{\pi^{\frac{1}{2}}}\int_0^\infty \frac{P_m(E,\tau)}{(k_B T)^{\frac{3}{2}}} E^{\frac{1}{2}} e^{-\frac{E}{k_B T}} dE. \quad (14)$$

Here we define the fraction of molecules formed (assuming an equal number of initial atoms of different species), after a square pulse of duration τ, to be given simply by

$$\frac{N_m}{N_a} = \langle P_m(T,\tau)\rangle. \quad (15)$$

We note that, after the association pulse is applied, dynamical effects can arise due to photon recoil of the atoms and molecules leading to additional molecular association and heating [82]. However, in contrast to photoassociation, this effect should be negligible for our scheme, as the RF photon recoil energies are many orders of magnitude smaller than even the picokelvin temperature regime relevant to near-term studies in microgravity.

For molecular dissociation, our scheme is represented in Fig. 2(b), leading us to set $E_k = 0$ and $E_m = E + \Delta E - E_b - i\hbar\gamma/2$ in Eq. (10). Therefore, similarly to association, we now consider the solutions of Eq. (10) and assume that the system is found in the molecular state ($\nu = m$) at $t = 0$. The probability of finding the system in the unbound state ($\nu = k$) at later times, τ, is

$$P_k(\delta,\tau) = e^{-\gamma\tau/2}\left(\frac{\Omega_m}{\Omega^k_{\rm eff}}\right)^2 \left|\sin\left(e^{i\theta_k}\frac{\Omega^k_{\rm eff}\tau}{2}\right)\right|^2, \quad (16)$$

where

$$\Omega^k_{\rm eff} = \left[\gamma^2\delta^2 + \left(\Omega_m^2 + \delta^2 - \frac{\gamma^2}{4}\right)^2\right]^{\frac{1}{4}}, \quad (17)$$

$$\theta_k = \frac{1}{2}\tan^{-1}\left[\frac{\delta\gamma}{\Omega_m^2 + \delta^2 - \frac{\gamma^2}{4}}\right]. \quad (18)$$

Here, we note that the energy of the dissociated atoms is given by the energy detuning $\hbar\delta$ [see Fig. 2(b)]. As a result, for dissociation the k dependence of Ω_m in Eq. (9) needs to be replaced by the wave number associated with the energy detuning, $k_\delta^2 = 2\mu\delta/\hbar$, i.e., the relevant Rabi frequency is now dependent on the detuning, $\Omega_m \equiv \Omega_m(\delta)$. We also note that, for molecular dissociation, thermal effects can only be introduced via the Doppler effect, i.e., molecules with different velocities will experience a different external-field frequency, $\omega/2\pi$. However, the fact that we assume low temperatures and low-frequency transitions effectively negates the effects of Doppler broadening in dissociation (see Sec. III B). In that case, the fraction of atoms formed after a square pulse of duration τ is given simply by

$$\frac{N_a}{N_m} = P_k(\delta,\tau). \quad (19)$$

Among the conditions for the validity of the above approach, the requirement that the system is found in the dilute regime, i.e., $na^3 \ll 1$ and $na'^3 \ll 1$, is of crucial importance. If such conditions are not satisfied, nontrivial finite-density effects have to be considered, which is beyond the capability of our current model. Our model also requires that $\hbar\Omega_m/E_b \ll 1$ in order to avoid free-to-free transitions during both association and dissociation as well as multiphoton effects. Although our model could be extended in order to properly include such effects, it is of experimental interest to restrict ourselves to parameters in which $\hbar\Omega_m/E_b \ll 1$ since this is the regime in which one can associate or dissociate Feshbach molecules more efficiently and without generating significant heating.

III. RESULTS AND DISCUSSION

The focus of this study is to explore association and dissociation of heteronuclear Feshbach molecules in the parameter regime relevant for CAL, i.e., we consider temperatures at or below 1 nK and atomic densities as low as $n_{\rm K} = n_{\rm Rb} = 10^8/{\rm cm}^3$. We show that this low-temperature and low-density regime makes it possible to observe efficient association and dissociation as well as their corresponding coherent properties. For the present studies, we consider fields which are far detuned from the atomic transition, i.e., $\hbar\Omega/E_b \ll 1$. Ensuring that $\hbar\Omega/E_b$ is small prevents single-atom spin-flip transitions, which can reduce the number of atoms in the initial state for association: for the parameters used here for the atomic Rabi frequency and detunings we estimate a 4% probability of this effect (see Sec. III A).

In the following, we study the case where an RF field is applied to a heteronuclear mixture of ^{87}Rb and ^{41}K initially in the $|10\rangle$ and $|11\rangle$ states, respectively, with $\Omega/2\pi = 0.2$ kHz for Rb. Molecular association and dissociation are thereby induced at $a = 10^4 a_0$ ($E_b/h = 642.94$) Hz, assuming that $a' = 100a_0$ for the initial atomic state. Therefore, we are assuming bosonic heteronuclear Feshbach molecules which are about 10 times larger (and 100 times more weakly bound) than previously studied [62,63]. Here, three-body losses, which can play an important role at such large scattering lengths [23,24], will be greatly suppressed in the low-density, low-temperature regimes available at CAL. In fact, a detailed analysis of Refs. [83–85], along with some of the experimental data from Refs. [25] and [26], allows us to set $\gamma = 500$ mHz for this mixture, implying a molecular lifetime of about 2 s. This leaves plenty of time to associate and dissociate Feshbach molecules with minimal effects from loss.

A. Molecular association

Figure 3 shows our results for molecular association efficiency [Eq. (15)] after an RF pulse of duration τ, for temperatures ranging from 1 nK to 10 pK. For each panel in Fig. 3 we display a density plot showing the pulse length dependence of the molecular fraction as a function of the detuning, δ, and a plot of the corresponding result for a π pulse (square with $\tau = \pi/\Omega_m$). Note that, in Fig. 3, we show both the thermally averaged results for molecular association efficiency (solid red curve) and the nonaveraged results (dot-dashed green curve) in order to emphasize the importance of finite-temperature effects. As one can see, the Rabi-oscillation

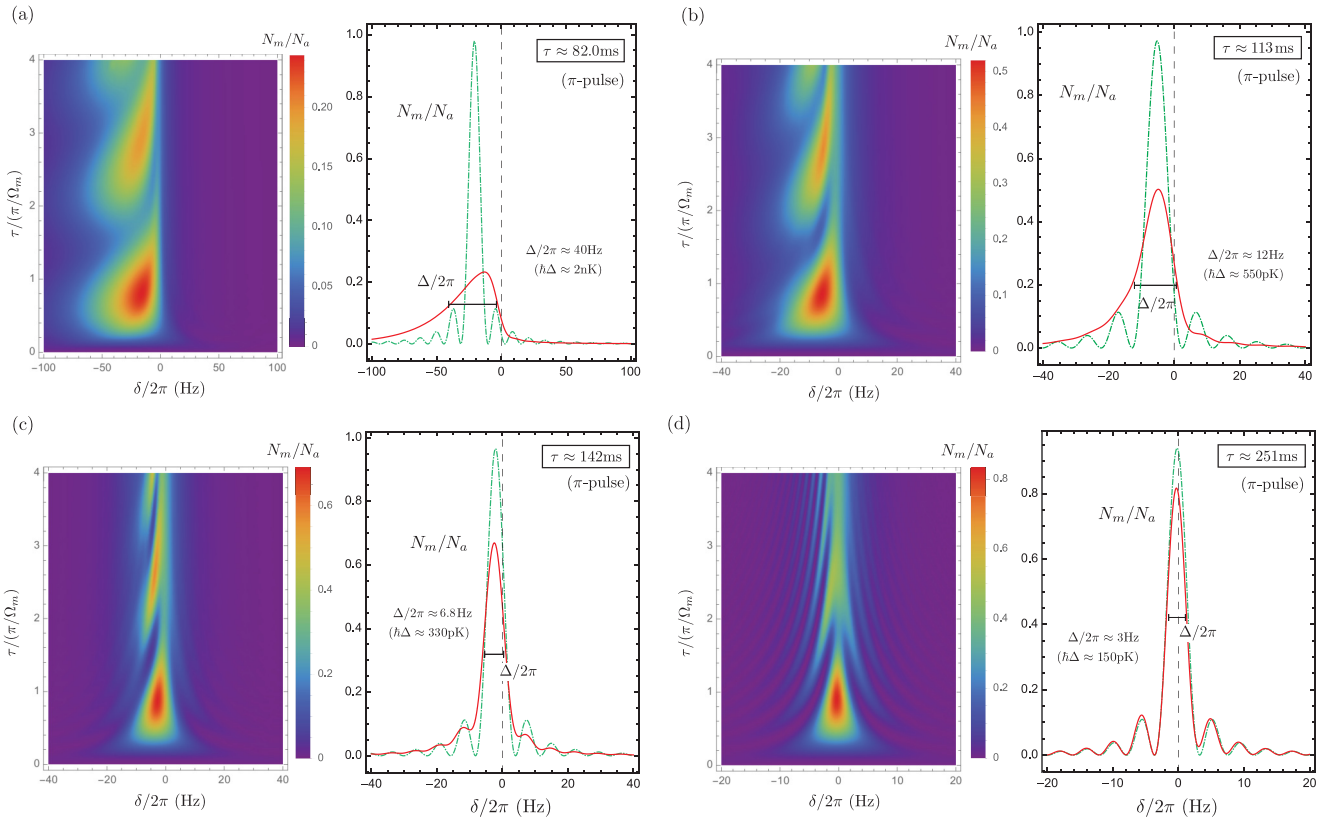

FIG. 3. Molecular association efficiency [Eq. (15)] for $a = 10^4 a_0$ ($E_b/h = 642.94$ Hz), $n = 10^8/\text{cm}^3$, $\Omega/2\pi = 0.2$ kHz, and different values of T and, consequently, Ω_m, as indicated. (a–d) Density plot showing the pulse length, τ, dependency of the molecular fraction as a function of the detuning, δ, and a figure for a π pulse ($\tau = \pi/\Omega_m$), displaying both the thermally averaged results [solid red curves given by Eq. (14)] and the nonaveraged results [dashed green curves given by Eq. (11), setting $E = k_B T$]. We indicate the values for the ratio $k_B T/\hbar\Omega_m$ characterizing the thermal regime as well as the association linewidth, $\Delta/2\pi$, which ultimately sets the temperature of the cloud after the pulse. Values of T/T_c: (a) $T/T_{c,\text{Rb}} \approx 25.3$ and $T/T_{c,\text{K}} \approx 11.4$, (b) $T/T_{c,\text{Rb}} \approx 6.33$ and $T/T_{c,\text{K}} \approx 2.84$, (c) $T/T_{c,\text{Rb}} \approx 2.53$ and $T/T_{c,\text{K}} \approx 1.14$, and (d) $T/T_{c,\text{Rb}} \approx 0.25$ and $T/T_{c,\text{K}} \approx 0.11$. The validity of the model as the system is cooled into the quantum-degenerate regime ($T/T_c < 1$) is discussed in Sec. III A. (a) $T = 1\text{nK}, \Omega_m/2\pi \approx 6.1$ Hz ($k_B T/\hbar\Omega_m \approx 3.42, \pi\gamma/2\Omega_m \approx 0.02$); (b) $T = 250\,\text{pK}, \Omega_m/2\pi \approx 4.4$ Hz ($k_B T/\hbar\Omega_m \approx 1.18, \pi\gamma/2\Omega_m \approx 0.03$); (c) $T = 100\,\text{pK}, \Omega_m/2\pi \approx 3.5$ Hz ($k_B T/\hbar\Omega_m \approx 0.59, \pi\gamma/2\Omega_m \approx 0.04$); (d) $T = 100\,\text{pK}, \Omega_m/2\pi \approx 2.0$ Hz ($k_B T/\hbar\Omega_m \approx 0.11, \pi\gamma/2\Omega_m \approx 0.06$).

line shape is almost completely washed out at high temperatures, while it is recovered in the low-temperature regime. In fact, for temperatures of 10 pK [Fig. 3(d)], atom-molecule coherences can be clearly seen, along with a high association efficiency.

In Fig. 3, the dimensionless quantity $k_B T/\hbar\Omega_m$, i.e., the ratio between the thermal energy and the energy associated with molecule-photon coupling, helps to define the regimes in which thermal effects are important. For $k_B T/\hbar\Omega_m > 1$ one would expect strong thermal effects since the atoms' motions are significant over the time scales for association. This behavior is clear in Fig. 3, where one can see that whenever $k_B T/\hbar\Omega_m > 1$ [Figs. 3(a) and 3(b)] the linewidth, $\Delta/2\pi$, is mainly determined by the temperature, while for $k_B T/\hbar\Omega_m < 1$ [Figs. 3(c) and 3(d)] it is determined by the molecular Rabi frequency. In fact, for $k_B T/\hbar\Omega_m < 1$, one can show from Eq. (11), neglecting loss effects, that the linewidth is approximately given by

$$\frac{\Delta}{2\pi} \approx 2\left(\frac{2}{\pi}\right)^{1/2} \frac{\Omega_m}{2\pi}. \tag{20}$$

Note that $\hbar\Delta$ will ultimately set the temperature of the molecular cloud after the pulse. Therefore, besides enabling a higher efficiency for association, it is also of experimental interest to keep Ω_m small so that minimal heating is introduced in the system. Doing so, however, implies that longer π pulses are necessary for association, which must be balanced with the time scales associated with losses.

One needs to combine low thermal broadening and minimal atomic losses to realistically observe efficient molecular association and atom-molecule coherent effects. These conditions are given by

$$\frac{k_B T}{\hbar\Omega_m} \approx \frac{0.54}{\alpha}\left[\frac{\mu^{3/4} a^{1/2} (k_B T)^{3/4}}{\hbar^{3/2} n^{1/3}}\right] \ll 1, \tag{21}$$

$$\frac{\pi\gamma}{2\Omega_m} \approx \frac{0.85}{\alpha}\left[\frac{\tilde{\gamma}\hbar^{1/2} n^{2/3} a^{3/2}}{(k_B T)^{1/4} \mu^{1/4}}\right] \ll 1, \tag{22}$$

where we have assumed $ka \ll 1$ and $\hbar\Omega/E_b = \alpha$ in Eq. (9), with $\alpha < 1$ as required for suppression of spin-flip transitions

For the ^{87}Rb-^{41}K system considered, $\alpha \approx 0.31$, leading to a 4% probability of loss from spin flips. In Eq. (22) we define the loss rate as $\gamma = \tilde{\gamma}(\hbar n a/\mu)$, with $\tilde{\gamma}$ given in terms of the few-body physics controlling atomic and molecular losses [24]—in our case, $\gamma = 500$ mHz, which leads to $\tilde{\gamma} \approx 4.2$. Note that, in the limit of low losses, Eq. (22) relates to the fraction of atoms remaining after a π pulse, $\exp(-\pi\gamma/2\Omega_m)$ [see Eq. (11)]. Therefore, Eqs. (21) and (22) can be used as a guide in order to understand the complex parameter regime that leads to the suppression of thermal effects combined with long lifetimes. In fact, based on our numerical calculations, we note that systems with the same value of $k_B T/\hbar\Omega_m$ and $\pi\gamma/2\Omega_m$ share the same degree of thermal and loss effects.

The optimal set of parameters will, however, be determined from the combination of low temperatures and densities based on how strong thermal and loss effects depend on these parameters. For instance, from Eq. (21), it is clear that thermal effects are more sensitive to temperature than density. [The opposite is true for loss effects from Eq. (22).] In order to illustrate how to achieve an optimal set of parameters we start from typical values for ground-based experiments [62,63]: $T = 100$ nK, $n = 10^{12}/\text{cm}^3$, $a = 800a_0$, and $\Omega = 50$ kHz. In this case, although losses are not as drastic, $\pi\gamma/2\Omega_m \approx 0.05$ ($\gamma = 400$ Hz [83–85]), thermal effects can be significant since $k_B T/\hbar\Omega_m \approx 1$. Although reducing the temperature to 1 nK strongly reduces thermal effects, $k_B T/\hbar\Omega_m \approx 0.03$, losses now can be important, $\pi\gamma/2\Omega_m \approx 0.15$, but not *drastically* important. If now the density is also decreased by a factor of 10, both thermal and loss effects should be suppressed ($k_B T/\hbar\Omega_m \approx 0.07$ and $\pi\gamma/2\Omega_m \approx 0.03$). We note, however, that this regime can only be achieved for these temperatures and densities because the assumed scattering length ($a = 800a_0$) is not as large. As shown in our results in Fig. 3, and according to Eqs. (21) and (22), as one assumes larger values of a, a high efficiency can only be accomplished by reducing temperatures and densities drastically. It is interesting to note that since $\Delta \propto \Omega_m$ [see Eq. (20)] one can increase a, and provided that all other relevant parameters are such that $k_B T/\hbar\Omega_m$ remains the same, the relative heating $\hbar\Delta/k_B T$ will also be the same.

The effects of quantum degeneracy might also be important at such low temperatures for parameters used in our calculations ($a = 10^4 a_0$ and $n = 10^8/\text{cm}^3$) given in Fig. 3. The critical temperature for condensation is about $T_{c,\text{Rb}} \approx 40$ pK and $T_{c,\text{K}} \approx 90$ pK for ^{87}Rb and ^{41}K, respectively [see specific values of T/T_c ($T_c \approx 3.31\hbar^2 n^{2/3}/m$) in the caption to Fig. 3]. In the context of molecular association, this means that atoms in the initial state will have a narrower energy distribution than a simple thermal cloud. As a result, the thermal effects displayed in our calculations for when $T/T_c < 1$ should be minimized, thus improving molecular conversion efficiency. For instance, the thermally averaged results [see Eq. (14)] in Figs. 3(c) and 3(d) should approach the nonaveraged results [see Eq. (11)] as the system enters into the quantum degenerate regime. This expected improvement of molecular association in the quantum degenerate regime has been verified experimentally in Refs. [86–88] and analyzed in Refs. [65] and [89]. To emphasize the importance of quantum degeneracy, we can recast the results in Eqs. (21) and (22) in terms of $T/T_c = T/T_{c,\text{K}} = (m_\text{K}/m_\text{Rb})T/T_{c,\text{Rb}}$, leading to

$$\frac{k_B T}{\hbar\Omega_m} \approx \frac{1.33}{\alpha}\left[\frac{(T/T_c)^{3/4}(na^3)^{1/6}}{(m_\text{K}/\mu)^{3/4}}\right] \ll 1, \tag{23}$$

$$\frac{\pi\gamma}{2\Omega_m} \approx \frac{0.63}{\alpha}\left[\frac{\tilde{\gamma}(na^3)^{1/2}}{(\mu/m_\text{K})^{1/4}(T/T_c)^{1/4}}\right] \ll 1 \tag{24}$$

and showing the reduction in thermal effects as T/T_c decreases, while loss effects are kept under control due to the weaker dependence in Eq. (24) on T/T_c. We also look for possible mean-field effects that can lead to collisional frequency shifts. In our case, however, the collisional frequency shift nU_0/h (where $U_0 = 2\pi\hbar^2 a'/\mu$, assuming $a' = 100a_0$) is about 0.001 Hz, and according to the results in Fig. 3 this would lead to small effects; this is also to be compared to the local energy $\epsilon_r/h \approx 5.9$ Hz, as determined from the discussion preceding Eq. (9) as well as the thermal energy, $k_B T/h \approx 0.2$ Hz (for $k_B T = 10$ pK). More generally, one can assume that whenever $na^3 \ll 1$ many-body effects should be suppressed. (In our studies we have $na'^3 \approx 10^{-11}$ and $na^3 \approx 10^{-5}$.) Nevertheless, it would be interesting to investigate many-body phenomena, such as rogue dissociation [90–93], in the realm of RF association employed here. (However, we expect such effects to be small within the parameter regime available at CAL.) In this case, a more sophisticated model for a dual-species condensate would be required and thus a precise analysis of such effects falls beyond the scope of the present study.

B. Molecular dissociation

Figure 4 shows results for the molecular dissociation efficiency [Eq. (19)], also assuming a density of $10^8/\text{cm}^3$, scattering length of $10^4 a_0$, and Rabi frequency $\Omega/2\pi = 0.2$ kHz. In Fig. 4(a) the density plot shows both the pulse length, τ, and detuning, δ, and the dependency of the fraction of atoms created after the dissociation pulse, with Rabi oscillations characterizing the coherent aspects of this process. In Figs. 4(b) and 4(c), we show the fraction of dissociated atoms for a fixed pulse length $\tau = 25$, 100, and 250 ms, respectively. The asymmetric profile of the dissociation line shape is the result of the dependence of the Rabi frequency $\Omega_m/2\pi$ on δ [see discussion followed by Eq. (16)]. As indicated in Figs. 4(b) and 4(c), this dependence causes the dissociation probability in Eq. (19) to vanish as $\delta^{1/2}$ for small δ and as $\delta^{7/2}$ for large δ, resulting in a asymmetric line shape.

It is important to note that, while for association one expects to obtain the maximum efficiency for a π pulse ($\tau = \pi/\Omega_m$) at $\delta \approx 0$, for dissociation (due to the dependence of Ω_m on δ) one now wants to know the detuning leading to maximum dissociation for a given pulse length as well as the corresponding width of the dissociation line shape, since this will ultimately determine the energy of the dissociated atomic pair. As one can see in Fig. 4(a), there is a characteristic pulse length, τ_c, beyond which dissociation becomes efficient and the corresponding linewidth becomes narrow. [See horizontal dashed line in Fig. 4(a).] One can show that this characteristic

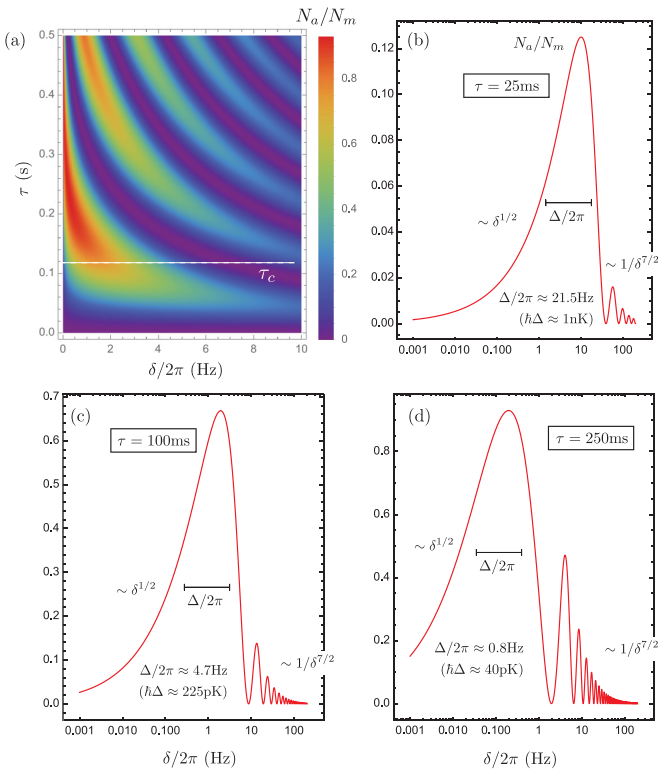

FIG. 4. Molecular dissociation efficiency [see Eq. (19)]: (a) as a function of the pulse duration and detuning and (b)–(d) for a fixed pulse duration. For longer pulses we obtain a high efficiency and a narrow linewidth, $\Delta/2\pi$.

time scale is given by

$$\tau_c = \frac{\hbar^{5/3}\pi^{5/3}}{4[a^2(a-a')^4\epsilon_r^2\mu^3\Omega^4]^{1/3}} \approx \frac{1.11}{\alpha^{4/3}}\left(\frac{\mu\, a^{2/3}}{\hbar\, n^{4/9}}\right), \quad (25)$$

where we have assumed $\alpha = \hbar\Omega/E_b < 1$ in order to ensure the suppression of spin-flip transitions. (For the parameters used in our calculations in Fig. 4 we obtain $\tau_c \approx 93$ ms.) For long pulses, i.e., for $\tau \gg \tau_c$, the value of the detuning in which the dissociation probability is maximized and the corresponding linewidth is given, respectively, by

$$\frac{\delta_{\max}}{2\pi} \approx \frac{\hbar^5\pi^5}{64a^2(a-a')^4\epsilon_r^2\mu^3\Omega^4}\frac{1}{\tau^4} \approx \frac{1.33}{\alpha^4}\frac{\mu^3a^2}{\hbar^3n^{4/3}}\left(\frac{1}{\tau^4}\right), \quad (26)$$

$$\frac{\Delta}{2\pi} \approx 5\frac{\delta_{\max}}{2\pi} \approx \frac{6.63}{\alpha^4}\frac{\mu^3a^2}{\hbar^3n^{4/3}}\left(\frac{1}{\tau^4}\right). \quad (27)$$

It is interesting to note that for $\tau \gg \tau_c$ the linewidth $\Delta \sim 1/\tau^4$ rapidly decreases as a function of the pulse length. In contrast, for shorter pulses, i.e., for $h/E_b \ll \tau \ll \tau_c$, the dissociation probability is drastically reduced and with line-shape parameters given by

$$\frac{\delta_{\max}}{2\pi} \approx \frac{2}{\tau}\left(\frac{3}{5}\right)^{1/2} \quad \text{and} \quad \frac{\Delta}{2\pi} \approx \frac{1}{4}\left(\frac{5}{3}\right)^{1/2}\frac{\delta_{\max}}{2\pi}. \quad (28)$$

Therefore, for short pulses, since $\Delta/2\pi \sim 1/\tau$, one would expect broad line shapes and, consequently, substantially more heating than for long pulses. We note that our results for both long and short pulses lead to $\Delta/2\pi \sim \delta_{\max}/2\pi$, which is in agreement with the experimental findings in Ref. [30]. We also note that although our longest ($\tau = 250$ ms) and shortest ($\tau = 25$ ms) pulse lengths are not strongly in the $\tau \gg \tau_c$ and $\tau \ll \tau_c$ regimes, we still obtain a reasonable agreement between our numerical results for $\delta_{\max}/2\pi$ and $\Delta/2\pi$ and those from Eqs. (26)–(28).

Based on this analysis, it is clear that the conditions for efficient dissociation relies on the pulse length as well as the time scale for molecular losses. These conditions can be expressed as

$$\frac{\tau_c}{\tau} \approx \frac{1.11}{\alpha^{4/3}}\left(\frac{\mu\, a^{2/3}}{\hbar\, n^{4/9}}\right)\frac{1}{\tau} \ll 1, \quad (29)$$

$$\frac{\gamma\tau}{2} \approx \frac{\tau}{2}\left(n\tilde{\gamma}\frac{\hbar a}{\mu}\right) \ll 1. \quad (30)$$

For instance, from the above equations we can see that although increasing the density improves the condition for long pulses [Eq. (29)], it can lead to stronger losses [Eq. (30)]. In fact, based on the different dependences on the experimentally relevant parameters in Eqs. (29) and (30), one can draw general conclusions concerning dissociation efficiency in different regimes. For high densities, for instance, Eqs. (29) and (30) indicate that efficient dissociation can only be achieved for small values of a, in order to minimize loss effects. On the other hand, Eqs. (29) and (30) also indicate that dissociation of very weakly bound Feshbach molecules (large a) can only be efficient if one now considers the regime of both low density and long pulses. We note that, differently from association, increasing a could in principle lead to a broader linewidth ($\Delta/2\pi \sim a^2$) [see Eq. (27)], resulting in dissociated atoms with a higher kinetic energy $\hbar\Delta$ [30]. However, due to the strong dependency of $\Delta/2\pi$ on τ, it turned out to be much easier to obtain narrow linewidths for dissociation than for association.

As mentioned in Sec. II—the discussion following Eq. (16)—thermal effects in molecular dissociation can only be introduced via the Doppler effect. For the parameters relevant to our problem, however, Doppler broadening, $\Delta\omega = \omega(k_BT/mc^2)^{1/2}$, is found to be negligible. For instance, for ^{87}Rb the resonant frequency $\omega/2\pi$ for the transition $|10\rangle$-$|11\rangle$ is less than 30 MHz for fields below 40 G, which corresponds to Doppler widths below 0.05 mHz at $T = 1$ nK. Nevertheless, for dissociation one could expect very narrow linewidths for long pulses ($\tau \gg \tau_c$), and the Doppler broadening will, at some point, be the main factor determining the linewidth for molecular dissociation. Similar to the case of association, molecular dissociation could also be sensitive to mean-field shifts (estimated above to be of the order of 0.1 Hz). In the regime of long dissociation pulses, $\tau \gg \tau_c$, leading to very narrow linewidths (see Fig. 4), mean-field shifts can in fact become important in determining the value of the detuning in which dissociation is maximum. However, in order to more precisely determine these mean-field shifts one would need to explore in detail the nature of the molecule-molecule interactions and their universal properties [94,95], a task beyond the scope of the present study.

IV. SUMMARY

We have developed a simple theoretical model capable of describing association and dissociation of weakly bound heteronuclear Feshbach molecules with oscillating, state-changing fields. Our model accounts for coherent Rabi oscillations within times scales shorter than $2\pi/\Omega_m$ (which, incidentally, would be damped on one side of the resonance by the coupling to the continuum) and also qualitatively includes incoherent phenomena associated with atomic and molecular losses. Our analysis shows that the ultralow temperature and density regimes expected at CAL are beneficial for studies of association and dissociation of Feshbach molecules as well as the coherent properties of these processes. Hence, not only is the typical utility of Feshbach molecular physics enhanced in space, but also new applications emerge. Notably, heteronuclear Feshbach molecules can be used to achieve exquisite control over the initial density and momentum states of dual-species atomic and molecular gases for space-based fundamental physics research [96]. We note that, in most of our calculations, the effects of the losses are suppressed due to the low-density regime accessible at CAL. Nevertheless, it would be interesting to explore experimentally the regime in which losses are important [63] in order to observe possible shifts of the association and/or dissociation linewidth due to losses, as predicted by Eqs. (11) and (16).

ACKNOWLEDGMENTS

This research was carried out under a contract with the National Aeronautics and Space Administration. M.K. acknowledges support by the German space agency with funds provided by the Federal Ministry of Economics and Technology under Grants No. 50WP1432, No. 50WM1132, and No. 1237. J.P.D. also acknowledges partial support from U.S. National Science Foundation Grant No. PHY-1307380.

[1] C. Chin, R. Grimm, P. S. Julienne, and E. Tiesinga, Rev. Mod. Phys. **82**, 1225 (2010).
[2] T. Köhler, K. Góral, and P. S. Julienne, Rev. Mod. Phys. **78**, 1311 (2006).
[3] M. Greiner, C. A. Regal, and D. Jin, Nature (London) **426**, 537 (2003).
[4] J. Cubizolles, T. Bourdel, S. J. J. M. F. Kokkelmans, G. V. Shlyapnikov, and C. Salomon, Phys. Rev. Lett. **91**, 240401 (2003).
[5] C. A. Regal, M. Greiner, and D. S. Jin, Phys. Rev. Lett. **92**, 083201 (2004).
[6] S. Jochim, M. Bartenstein, A. Altmeyer, G. Hendl, S. Riedl, C. Chin, J. H. Denschlag, and R. Grimm, Science **302**, 2101 (2003).
[7] M. W. Zwierlein, C. A. Stan, C. H. Schunck, S. M. F. Raupach, A. J. Kerman, and W. Ketterle, Phys. Rev. Lett. **92**, 120403 (2004).
[8] K. E. Strecker, G. B. Partridge, and R. G. Hulet, Phys. Rev. Lett. **91**, 080406 (2003).
[9] C. A. Regal, M. Greiner, and D. S. Jin, Phys. Rev. Lett. **92**, 040403 (2004).
[10] C. Chin, M. Bartenstein, A. Altmeyer, S. Riedl, S. Jochim, J. H. Denschlag, and R. Grimm, Science **305**, 1128 (2004).
[11] M. W. Zwierlein, J. R. Abo-Shaeer, A. Schirotzek, C. H. Schunck, and W. Ketterle, Nature (London) **435**, 1047 (2005).
[12] S. Ospelkaus, A. Pe'er, K.-K. Ni, J. J. Zirbel, B. Neyenhuis, S. Kotochigova, P. S. Julienne, J. Ye, and D. S. Jin, Nat. Phys. **4**, 622 (2008).
[13] K.-K. Ni, S. Ospelkaus, M. H. G. de Miranda, A. Pe'er, B. Neyenhuis, J. J. Zirbel, S. Kotochigova, P. S. Julienne, D. S. Jin, and J. Ye, Science **322**, 231 (2008).
[14] J. J. Zirbel, K.-K. Ni, S. Ospelkaus, J. P. D'Incao, C. E. Wieman, J. Ye, and D. S. Jin, Phys. Rev. Lett. **100**, 143201 (2008).
[15] C.-H. Wu, J. W. Park, P. Ahmadi, S. Will, and M. W. Zwierlein, Phys. Rev. Lett. **109**, 085301 (2012).
[16] M.-S. Heo, T. T. Wang, C. A. Christensen, T. M. Rvachov, D. A. Cotta, J.-H. Choi, Y.-R. Lee, and W. Ketterle, Phys. Rev. A **86**, 021602(R) (2012).
[17] S.-K. Tung, C. Parker, J. Johansen, C. Chin, Y. Wang, and P. S. Julienne, Phys. Rev. A **87**, 010702(R) (2013).
[18] M. Repp, R. Pires, J. Ulmanis, R. Heck, E. D. Kuhnle, M. Weidemüller, and E. Tiemann, Phys. Rev. A **87**, 010701(R) (2013).
[19] M. P. Köppinger, D. J. McCarron, D. L. Jenkin, P. K. Molony, H.-W. Cho, S. L. Cornish, C. R. LeSueur, C. L. Blackley, and J. M. Hutson, Phys. Rev. A **89**, 033604 (2014).
[20] F. Wang, D. Xiong, X. Li, D. Wang, and E. Tiemann, Phys. Rev. A **87**, 050702(R) (2013).
[21] T. Takekoshi, M. Debatin, R. Rameshan, F. Ferlaino, R. Grimm, H.-C. Nägerl, C. R. LeSueur, J. M. Hutson, P. S. Julienne, S. Kotochigova, and E. Tiemann, Phys. Rev. A **85**, 032506 (2012).
[22] B. Deh, W. Gunton, B. G. Klappauf, Z. Li, M. Semczuk, J. Van Dongen, and K. W. Madison, Phys. Rev. A **82**, 020701(R) (2010).
[23] E. Braaten and H.-W. Hammer, Phys. Rep. **428**, 259 (2006).
[24] Y. Wang, J. P. D'Incao, and B. D. Esry, Adv. At. Mol. Opt. Phys. **62**, 1 (2013).
[25] G. Barontini, C. Weber, F. Rabatti, J. Catani, G. Thalhammer, M. Inguscio, and F. Minardi, Phys. Rev. Lett. **103**, 043201 (2009).
[26] R. S. Bloom, M.-G. Hu, T. D. Cumby, and D. S. Jin, Phys. Rev. Lett. **111**, 105301 (2013).
[27] S.-K. Tung, K. Jiménez-García, J. Johansen, C. V. Parker, and C. Chin, Phys. Rev. Lett. **113**, 240402 (2014).
[28] R. Pires, J. Ulmanis, S. Häfner, M. Repp, A. Arias, E. D. Kuhnle, and M. Weidemüller, Phys. Rev. Lett. **112**, 250404 (2014).
[29] R. A. W. Maier, M. Eisele, E. Tiemann, and C. Zimmermann, Phys. Rev. Lett. **115**, 043201 (2015).
[30] M. Greiner, C. A. Regal, J. T. Stewart, and D. S. Jin, Phys. Rev. Lett. **94**, 110401 (2005).
[31] U. V. Poulsen and K. Mølmer, Phys. Rev. A **63**, 023604 (2001).
[32] K. V. Kheruntsyan and P. D. Drummond, Phys. Rev. A **66**, 031602(R) (2002).
[33] K. V. Kheruntsyan, Phys. Rev. A **71**, 053609 (2005).
[34] V. A. Yurovsky and A. Ben-Reuven, Phys. Rev. A **67**, 043611 (2003).
[35] C. M. Savage and K. V. Kheruntsyan, Phys. Rev. Lett. **99**, 220404 (2007).

[36] K. V. Kheruntsyan, M. K. Olsen, and P. D. Drummond, Phys. Rev. Lett. **95**, 150405 (2005).

[37] B. Zhao, Z.-B. Chen, J.-W. Pan, J. Schmiedmayer, A. Recati, G. E. Astrakharchik, and T. Calarco, Phys. Rev. A **75**, 042312 (2007).

[38] M. J. Davis, S. J. Thwaite, M. K. Olsen, and K. V. Kheruntsyan, Phys. Rev. A **77**, 023617 (2008).

[39] C. Gneiting and K. Hornberger, Phys. Rev. Lett. **101**, 260503 (2008).

[40] C. Gneiting and K. Hornberger, Phys. Rev. A **81**, 013423 (2010).

[41] C. Chin and V. V. Flambaum, Phys. Rev. Lett. **96**, 230801 (2006).

[42] C. Chin, V. V. Flambaum, and M. G. Kozlov, New J. Phys. **11**, 055048 (2009).

[43] A. Borschevsky, K. Beloy, V. V. Flambaum, and P. Schwerdtfeger, Phys. Rev. A **83**, 052706 (2011).

[44] M. Gacesa and R. Côté, J. Mol. Spectrosc. **300**, 124 (2014).

[45] *Recapturing a Future for Space Exploration: Life and Physical Sciences Research for a New Era*, National Research Council, Committee for the Decadal Survey on Biological and Physical Sciences in Space (The National Academies Press, Washington DC, 2011), p. 1.

[46] S. G. Turyshev, U. E. Israelsson, M. Shao, N. Yu, A. Kusenko, E. L. Wright, C. W. F. Everitt, M. Kasevich, J. A. Lipa, J. C. Mester, R. D. Reasenberg, R. L. Walsworth, N. Ashby, H. Gould, and H. J. Paik, Int. J. Mod. Phys. D **16**, 1879 (2007).

[47] D. A. Binns, N. Randoa, and L. Cacciapuoti, Adv. Space Res. **43**, 1158 (2009).

[48] H. Muntinga, H. Ahlers, M. Krutzik, A. Wenzlawski, S. Arnold, D. Becker, K. Bongs, H. Dittus, H. Duncker, N. Gaaloul, C. Gherasim, E. Giese, C. Grzeschik, T. W. Hansch, O. Hellmig, W. Herr, S. Herrmann, E. Kajari, S. Kleinert, C. Lammerzahl, W. Lewoczko-Adamczyk, J. Malcolm, N. Meyer, R. Nolte, A. Peters, M. Popp, J. Reichel, A. Roura, J. Rudolph, M. Schiemangk, M. Schneider, S. T. Seidel, K. Sengstock, V. Tamma, T. Valenzuela, A. Vogel, R. Walser, T. Wendrich, P. Windpassinger, W. Zeller, T. van Zoest, W. Ertmer, W. P. Schleich, and E. M. Rasel, Phys. Rev. Lett. **110**, 093602 (2013).

[49] T. van Zoest, N. Gaaloul, Y. Singh, H. Ahlers, W. Herr, S. T. Seidel, W. Ertmer, E. Rasel, M. Eckart, E. Kajari, S. Arnold, G. Nandi, W. P. Schleich, R. Walser, A. Vogel, K. Sengstock, K. Bongs, W. Lewoczko-Adamczyk, M. Schiemangk, T. Schuldt, A. Peters, T. Konemann, H. Muntinga, C. Lammerzahl, H. Dittus, T. Steinmetz, T. W. Hansch, and J. Reichel, Science **328**, 1540 (2010).

[50] G. Stern, B. Battelier, R. Geiger, G. Varoquaux, A. Villing, F. Moron, O. Carraz, N. Zahzam, Y. Bidel, W. Chaibi, F. P. Dos Santos, A. Bresson, A. Landragin, and P. Bouyer, Eur. Phys. J. D **53**, 353 (2009).

[51] N. Yu, J. M. Kohel, J. R. Kellogg, and L. Maleki, Appl. Phys. B **84**, 647 (2006).

[52] T. Schuldt, C. Schubert, M. Krutzik *et al.*, Exp. Astron. **39**, 167 (2015); D. N. Aguilera, H. Ahlers, B. Battelier *et al.*, Class. Quantum Grav. **31**, 115010 (2014).

[53] J. R. Williams, S.-w. Chiow, H. Müller, and N. Yu, New J. Phys. **18**, 025018 (2016).

[54] S. Chu, J. E. Bjorkholm, A. Ashkin, J. P. Gordon, and L. W. Hollberg, Opt. Lett. **11**, 73 (1986).

[55] H. Ammann and N. Christensen, Phys. Rev. Lett. **78**, 2088 (1997).

[56] S. H. Myrskog, J. K. Fox, H. S. Moon, J. B. Kim, and A. M. Steinberg, Phys. Rev. A **61**, 053412 (2000).

[57] A. E. Leanhardt, T. A. Pasquini, M. Saba, A. Schirotzek, Y. Shin, D. Kielpinski, D. E. Pritchard, and W. Ketterle, Science **301**, 1513 (2003).

[58] A. H. Hansen, A. Y. Khramov, W. H. Dowd, A. O. Jamison, B. Plotkin-Swing, R. J. Roy, and S. Gupta, Phys. Rev. A **87**, 013615 (2013).

[59] M. J. Davis and C. W. Gardiner, J. Phys. B **35**, 733 (2002).

[60] S.-w. Chiow, J. R. Williams, N. Yu, and H. Müller, arXiv:1612.02053v1 (2016).

[61] R. J. Thompson, Science Envelope Requirements Document (SERD) for Cold Atom Laboratory, JPL Technical Report (Jet Propulsion Laboratory, Pasadena, CA, 2013).

[62] C. Klempt, T. Henninger, O. Topic, M. Scherer, L. Kattner, E. Tiemann, W. Ertmer, and J. J. Arlt, Phys. Rev. A **78**, 061602(R) (2008).

[63] C. Weber, G. Barontini, J. Catani, G. Thalhammer, M. Inguscio, and F. Minardi, Phys. Rev. A **78**, 061601(R) (2008).

[64] C. Chin and P. S. Julienne, Phys. Rev. A **71**, 012713 (2005).

[65] T. M. Hanna, T. Köhler, and K. Burnett, Phys. Rev. A **75**, 013606 (2007).

[66] T. M. Hanna, E. Tiesinga, and P. S. Julienne, New J. Phys. **12**, 083031 (2010).

[67] P. Zhang, P. Naidon, and M. Ueda, Phys. Rev. Lett. **103**, 133202 (2009).

[68] T. V. Tscherbul, T. Calarco, I. Lesanovsky, R. V. Krems, A. Dalgarno, and J. Schmiedmayer, Phys. Rev. A **81**, 050701(R) (2010).

[69] D. J. Papoular, G. V. Shlyapnikov, and J. Dalibard, Phys. Rev. A **81**, 041603(R) (2010).

[70] Y. Ding, J. P. D'Incao, and C. H. Greene, arXiv:1607.01112.

[71] C. Klempt, T. Henninger, O. Topic, J. Will, W. Ertmer, E. Tiemann, and J. Arlt, Phys. Rev. A **76**, 020701(R) (2007).

[72] A. Simoni, M. Zaccanti, C. D'Errico, M. Fattori, G. Roati, M. Inguscio, and G. Modugno, Phys. Rev. A **77**, 052705 (2008).

[73] G. Thalhammer, G. Barontini, J. Catani, F. Rabatti, C. Weber, A. Simoni, F. Minardi, and M. Inguscio, New J. Phys. **11**, 055044 (2009).

[74] S.-I. Chu and D. A. Telnov, Phys. Rep. **390**, 1 (2004).

[75] K. Huang and C. N. Yang, Phys. Rev. **105**, 767 (1957).

[76] B. Borca, D. Blume, and C. H. Greene, New J. Phys. **5**, 111 (2003).

[77] K. Góral, T. Köhler, S. A. Gardiner, E. Tiesinga, and P. S. Julienne, J. Phys. B **37**, 3457 (2004).

[78] J. von Stecher and C. H. Greene, Phys. Rev. Lett. **99**, 090402 (2007).

[79] A. G. Sykes, J. P. Corson, J. P. D'Incao, A. P. Koller, C. H. Greene, A. M. Rey, K. R. A. Hazzard, and J. L. Bohn, Phys. Rev. A **89**, 021601(R) (2014).

[80] J. P. Corson and J. L. Bohn, Phys. Rev. A **91**, 013616 (2015).

[81] C. Cohen-Tannoudji, J. Dupont-Roc, and G. Grynberg, *Atom-Photon Interactions: Basic Processes and Applications* (John Wiley & Sons, New York, 1992).

[82] E. Luc-Koenig, F. Masnou-Seeuws, and R. Kosloff, Phys. Rev. A **76**, 053415 (2007).

[83] K. Helfrich, H.-W. Hammer, and D. S. Petrov, Phys. Rev. A **81**, 042715 (2010).

[84] J. P. D'Incao, H. Suno, and B. D. Esry, Phys. Rev. Lett. **93**, 123201 (2004).
[85] Y. Wang, J. Wang, J. P. D'Incao, and C. H. Greene, Phys. Rev. Lett. **109**, 243201 (2012).
[86] E. Hodby, S. T. Thompson, C. A. Regal, M. Greiner, A. C. Wilson, D. S. Jin, E. A. Cornell, and C. E. Wieman, Phys. Rev. Lett. **94**, 120402 (2005).
[87] S. T. Thompson, E. Hodby, and C. E. Wieman, Phys. Rev. Lett. **95**, 190404 (2005).
[88] S. B. Papp and C. E. Wieman, Phys. Rev. Lett. **97**, 180404 (2006).
[89] J. E. Williams, N. Nygaard, and C. W. Clark, New J. Phys **8**, 150 (2006).
[90] J. Javanainen and M. Mackie, Phys. Rev. Lett. **88**, 090403 (2002).
[91] T. Gasenzer, Phys. Rev. A **70**, 021603(R) (2004).
[92] P. Naidon and F. Masnou-Seeuws, Phys. Rev. A **73**, 043611 (2006).
[93] P. Naidon, E. Tiesinga, and P. S. Julienne, Phys. Rev. Lett. **100**, 093001 (2008).
[94] J. P. D'Incao, J. von Stecher, and C. H. Greene, Phys. Rev. Lett. **103**, 033004 (2009).
[95] J. P. D'Incao, S. T. Rittenhouse, N. P. Mehta, and C. H. Greene, Phys. Rev. A **79**, 030501(R) (2009).
[96] M. Krutzik, E. Elliott, J. R. Williams, and J. P. D'Incao (unpublished).